Int. J. Heat Mass Transfer. Vol. 30, No. 3, pp. 459–467, 1987
Printed in Great Britain

0017–9310/87 $3.00 + 0.00
Pergamon Journals Ltd.

A theoretical model of direct contact condensation on a horizontal surface

G. P. CELATA, M. CUMO, G. E. FARELLO and G. FOCARDI
ENEA—TERM/ISP Casaccia, Via Anguillarese 301, 00060 Rome, Italy

(*Received* 22 *April* 1986)

Abstract—With reference to the interaction between saturated steam and horizontal, subcooled, slowly moving water, a theoretical model of direct contact condensation is presented, for a cylindrical geometry. A good agreement appears from the comparison of predictions with experimental data, as far as both heat transfer coefficient and outlet water temperature are concerned.

1. INTRODUCTION

DIRECT contact heat transfer condensation is a phenomenon of fundamental importance as far as the safety analysis and industrial applications of LWRs are concerned. A typical nuclear situation could be the refill stage after a loss-of-coolant accident in a PWR, whereby the emergency cooling water (in a subcooled condition) comes into direct contact with the steam (in saturated or superheated condition), filling up the pressure vessel with the over heated core. Heat transfer characteristics, including thermal non-equilibrium effects, are not clear enough [1–13].

In this paper, referring to a previous experimental research [14], a model for direct contact condensation between saturated steam (in a quasi-stagnant situation) and subcooled (horizontally slowly flowing) water is shown. The experiments, contrary to the Nusselt theory, refer to a direct contact condensation situation in which a consistent and well-defined 'bulk region' takes place in the liquid phase.

A good agreement appears from the comparison of predictions with the experimental data [14]. Although the model has been developed for a particular (cylindrical) geometry, it can be easily extended to other ones. An extension to the plane geometry, together with *ad hoc* experiments will be accomplished in the near future.

2. REFERENCE GEOMETRY

The reference geometry is shown in Fig. 1. The test section employed in the experiments is made up of a cylindrical vessel with a flange at the bottom. The flange holds a Teflon cylindrical pool in which the water is allowed to flow radially. The water enters the bottom of the pool according to a circumferential distribution and, after the interaction with the steam, exits through a central discharge channel in order to be collected and 'processed', to obtain the measurement of the condensed mass flow rate.

The water discharge channel is kept 7.5 mm below the water level, so as to avoid steam leakages (carry-under). The water level is kept strictly constant over all the runs. This configuration enables us to schematize a simple geometry (a cylinder whose diameter is the pool inner diameter and whose height is the distance between the water surface and the water discharge channel), inside which the water may be supposed to flow horizontally and parallel to the water surface. The heat flux is therefore normal to the water motion. The steam enters the top of the test section, in order to get rid of the water convective heat transfer component.

3. PRELIMINARY REMARKS FOR THE MODEL DESCRIPTION

Analysing direct contact condensation data available in scientific literature, it appears evident that the heat transfer resistance lies only in a thin layer of water very close to the interface, unless a considerable amount of non-condensable gas is present. However, in the experiments, the presence of a non-condensable bleeder line allows the steam-side heat transfer resistance to be neglected; as a consequence, the interface can be considered at the saturation temperature, referred to the system pressure.

Concerning the steam–water dynamic interaction, the tests allow the effects of the steam kinematic characteristics to be neglected. As a matter of fact, the steam velocity is very low ($\sim 0.1\ \mathrm{m\,s^{-1}}$ maximum) and the flow is normal to the heat transfer surface; consequently the liquid turbulence is surely not dependent on steam motion. The above hypotheses have been systematically proved by experimental data, as the only parameter that turned out to be affecting the heat transfer was the superficial velocity of the water inside the pool, i.e. the inlet water mass flow rate and the level difference between the heat transfer surface and the discharge channel.

NOMENCLATURE

a_i	constants
A	cross-sectional area, integration constant
b	reversal region thickness
B	integration constant
c_p	specific heat
D	diameter, characteristic dimension
f_f	aspect factor
g	gravity acceleration, r and z function
h	heat transfer coefficient
H	enthalpy
K	thermal conductivity
P	perimeter, exchanged power
Pr	Prandtl number
r	radius, coordinate
r^*	characteristic radius (integration constant)
R	pool inner diameter
Re	Reynolds numbers
S	heat transfer surface
$T, \Delta T$	temperature, temperature difference
u	integration variable
v	velocity
v_o	parameter defined in equation (5)
W	mass flow rate
z	coordinate.

Greek symbols

β	parameter defined in equation (12')
γ_s	specific mass flow rate
δ_z	thermal boundary layer
θ	coordinate
λ	latent heat
μ	dynamic viscosity
ρ	density
σ	Gaussian distribution parameter.

Subscripts

act	actual
c	condensation
eq	equivalent
i	inlet
o	outlet
sat	saturation
t	total
turb	turbulent
v	vapour (saturated).

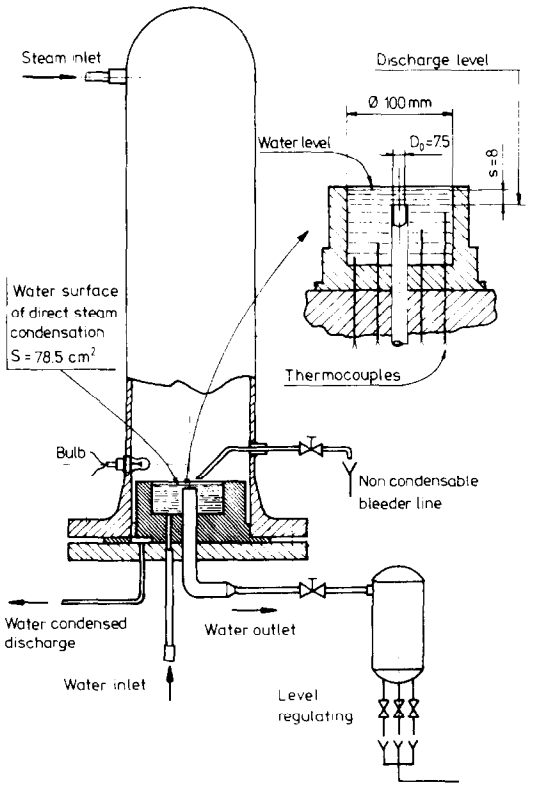

FIG. 1. Schematic diagram of the test section.

Under these premises and with reference to the described geometry, it is possible to represent the direct contact condensation phenomenon by the knowledge of the thermal field inside the pool, coupled with a fluid-dynamics model.

4. THE FLUID-DYNAMICS MODEL

In Fig. 2 a cutaway view of the pool is drawn, in which four characteristic regions of the fluid-dynamics field have been sketched.

I—Inlet region

This is characterized by the presence of six water diffusers, the task of which is to generate a uniform distribution of the water mass flow rate inside the pool, and to prevent the formation of waves on the heat transfer surface as well. The velocity field is not characterized by a preferential direction, with high mixing of the liquid.

II—Settling region

A transition region in which the liquid, from the mixing inlet, is pushed in a vertical bulk motion.

III—Uniform region

In this region the fluid motion is characterized by a typical vertical and uniform bulk velocity. Mixing streams, if present, are only due to thermal and kinetic diffusivity of the fluid (microvorticity) and not to the bulk motion.

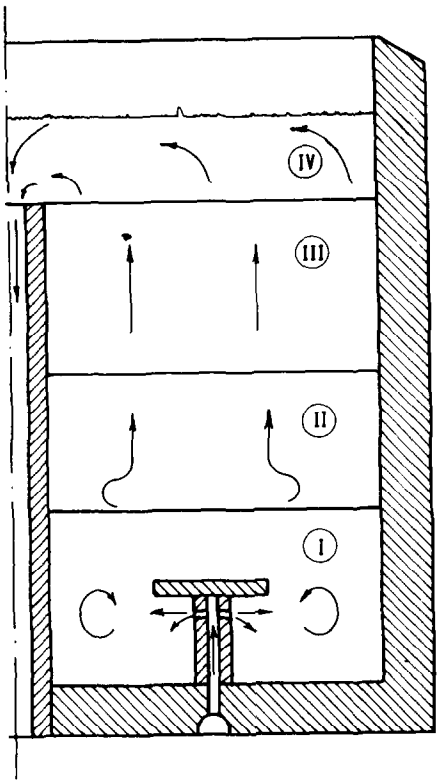

FIG. 2. Schematic diagram of the four fluid-dynamics regions.

IV—Reversal region

In this region the fluid changes the main velocity direction from vertical (upwards) to horizontal, towards (radially) the central outlet. It is, practically, the key region for the heat transfer; in fact, the steep thermal gradient layer which controls the direct contact condensation is contained inside this region, and its characteristics are determined only by the velocity field.

With reference to cylindrical coordinates (positive z-direction is downwards and coincident with the pool axis of symmetry), with the origin on the water surface, the water velocity vectorial field is expressed by

$$\mathbf{v} = v_z(r,\theta,z)\mathbf{u}_z + v_r(r,\theta,z)\mathbf{u}_r + v_\theta(r,\theta,z)\mathbf{u}_\theta \qquad (1)$$

where $\mathbf{u}_z$, $\mathbf{u}_r$, and $\mathbf{u}_\theta$ are the versors of the respective axes.

To solve the velocity field, the following simplifying hypotheses have been introduced.

(a) For symmetry:

$$\frac{\partial v_z}{\partial \theta} = \frac{\partial v_r}{\partial \theta} = \frac{\partial v_\theta}{\partial \theta} = 0$$

and, further, $v_\theta = 0$.

(b) In the reversal region it is possible to assume:

$$\frac{\partial v_r}{\partial z} = 0$$

with v_r considered equal to the average value in z.

(c) The z-component of velocity is not dependent on the r-coordinate:

$$\frac{\partial v_z}{\partial r} = 0.$$

(d) The thickness of the reversal region is not dependent on the r-coordinate:

$$h(r) = b.$$

(e) The mass flow rate is uniformly distributed over the base surface of the uniform region.

(f) The condensed flow rate is uninfluential from the fluid-dynamics viewpoint (it is less than 1% of the inlet water mass flow rate).

Owing to hypothesis (e) further conditions may be assumed (in the uniform region):

$$\frac{\partial v_z}{\partial r} = \frac{\partial v_z}{\partial z} = \frac{\partial v_z}{\partial \theta} = 0.$$

With r_o the outer diameter of the discharge channel and R the inner diameter of the pool, the specific vertical upward flow rate (III or 'uniform' region) is constant and expressed by

$$\gamma_s = \frac{W_i}{\pi(R^2 - r_o^2)}$$

where W_i is the inlet water mass flow rate.

With reference to the reversal region, the radial mass flow rate crossing the lateral surface of the generic cylinder (radius r) is given by (Fig. 3)

$$W(r) = \pi\gamma_s(R^2 - r^2) = W_i\frac{R^2 - r^2}{R^2 - r_o^2}. \qquad (2)$$

Finally, with hypothesis (d), the radial component of velocity (average value over the reversal region thickness) is expressed as a function of the radius

$$\bar{v}_r(r) = v_r(r,z) = \frac{W(r)}{2\pi r b\rho}. \qquad (3)$$

Remembering equation (2), $\bar{v}_r(r)$ can be written in the following form

$$\bar{v}_r(r) = v_r(r,z) = -v_o\left(\frac{R^2}{r} - r\right) \qquad (4)$$

with

$$v_o = \frac{W_i}{2\pi b\rho(R^2 - r_o^2)}. \qquad (5)$$

Applying the mass conservation equation to the infinitesimal cylindrical volume element (Fig. 4)

$$\frac{\partial v_r}{\partial r} + \frac{v_r}{r} = -\frac{\partial v_z}{\partial z}. \qquad (6)$$

Substituting expressions (4) and (5) in equation (6) gives

$$-\frac{\partial v_z}{\partial z} = 2v_o. \qquad (7)$$

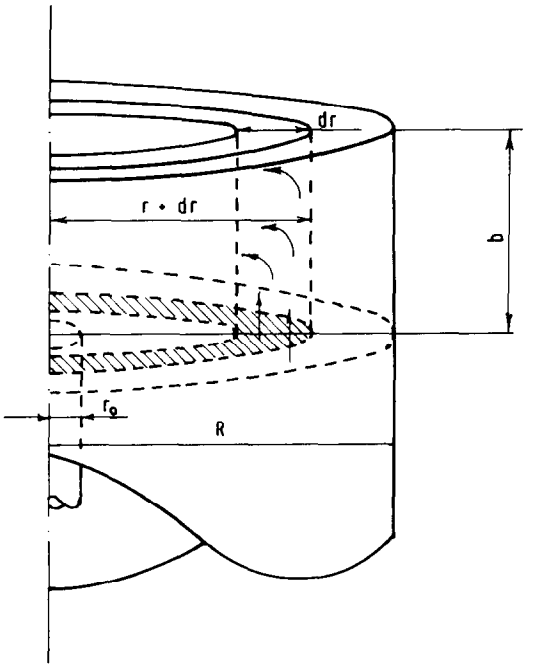

FIG. 3. Schematic diagram of the reversal region.

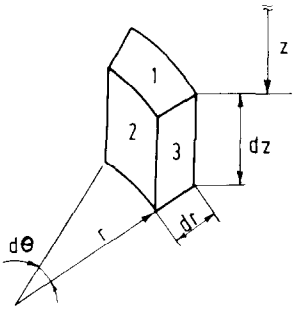

FIG. 4. The infinitesimal cylindrical volume element.

Integrating with the boundary condition $v_z(r,0) = 0$ (the vertical component of the velocity vanishes at the water surface)

$$v_z(z) = -2v_0 z. \tag{8}$$

In conclusion, the velocity field (1) in the reversal region has the following expression

$$\mathbf{v}(r,z) = -v_0\left[\left(\frac{R^2}{r} - r\right)\mathbf{u}_r + 2z\mathbf{u}_z\right]. \tag{9}$$

5. THE THERMAL MODEL

Let us now introduce the thermal model considering the water velocity to be so low that heat diffusion takes place by conduction and mass transport and not by turbulent diffusion, i.e. water laminar flow. We therefore neglect for the moment the typical effect of the turbulent regime for which the fluid seems to increase its own thermal conductivity. Such an effect is a sort of microscopic transport, but is quite different from the real transport [15]. Anyway, a more detailed analysis will be accomplished later. In a geometry, like the tested one [14], characterized by a heat transfer towards a water layer in non-turbulent motion perpendicular to the heat flux, the temperature gradient is confined to within a few millimetres of the water side (sometimes less than a millimetre). This is due to the low water thermal conductivity (at ambient temperature and pressure, about $0.5\,\mathrm{W\,°C^{-1}\,m^{-1}}$).

It is reasonable to suppose, as experimentally confirmed, that the thermal layer thickness, in which the temperature drop is concentrated, is less than the extension of the reversal region (see Fig. 2).

Remembering that, from energy balances, the total and condensation heat transfer coefficients are linked by the equation [14]

$$h_c = \frac{h_t}{[1 + (H_{lsat} - H_o)/\lambda]} \tag{10}$$

the following considerations are referred to the total heat transfer coefficient, h_t, physically more interesting as it takes into account all the heat transferred to the cooling water. This will be easily computed knowing the thermal field at the interface, $T = T(r,z,\theta)$.

With the thermal resistance being practically confined to the water side, referring to the liquid phase, Fourier's law yields

$$h_t = -\frac{K}{\Delta T}\frac{\partial T}{\partial Z}\bigg|_{z=0}$$

where $\Delta T = T_v - T_i$ is the condensation heat transfer driving force.

Obviously, h_t is a function of the r-coordinate, whilst it is not dependent, for symmetry, on the θ-coordinate.

In computing the thermal field, as the temperature is not constant, the physical properties of water have been evaluated at an average temperature, as suggested in Appendix A.

Referring again to the infinitesimal cylindrical volume element (Fig. 4), and considering as positive the heat entering this control volume, a heat balance (conduction and transport) coupled with the continuity equation (6), yields

$$K\frac{\partial^2 T}{\partial z^2} = \rho c_p\left(v_z\frac{\partial T}{\partial z} + v_r\frac{\partial T}{\partial r}\right). \tag{11}$$

To get equation (11), the radial conduction has been neglected (the radial temperature gradient is small) together with the heat transfer in the θ-direction (for symmetry).

Substituting equations (4) and (8) in equation (11)

$$\beta\frac{\partial^2 T}{\partial z^2} = -\frac{\partial T}{\partial r}\left(\frac{R^2}{r} - r\right) - 2z\frac{\partial T}{\partial z} \tag{12}$$

with

$$\beta = \frac{K}{\rho c_p v_0}.$$

The thermal field is a function of the r- and z-coordinates and is restricted between the saturation temperature, T_v, and the inlet water temperature, T_i. It is convenient to express the thermal field in terms of a temperature difference between the actual temperature, $T_{act}(r, z)$, and the inlet water temperature, T_i

$$T(r, z) = T_{act}(r, z) - T_i. \tag{13}$$

The general solution, physically congruent, of the partial differential equation (12) of parabolic type, is given by [16]

$$T(r, z) = A + B\int_0^g e^{-u^2}\,du \tag{14}$$

with

$$g = \frac{z}{z^*}\frac{(R^2 - r^2)/r^{*2}}{\sqrt{\left(\left(\frac{R^2 - r^2}{r^{*2}}\right)^2 + 1\right)}} \tag{15}$$

and

$$z^* = \sqrt{\beta} = \sqrt{\left(\frac{K}{\rho c_p v_0}\right)} \tag{16}$$

integration constants, A, B and r^*, may be determined with the boundary conditions.

The first two boundary conditions may be quickly deduced.

(1) Neglecting (see Section 3) the steam-side thermal resistance

$$T(r, 0) = T_v - T_i = T = A. \tag{17}$$

(2) Considering the thickness of the steep temperature drop water layer (a few millimetres):

$$\lim_{z\to\infty} T(r, z) = T + B\frac{\sqrt{\pi}}{2} = 0 \tag{18}$$

and then

$$B = -\frac{2}{\sqrt{\pi}}T. \tag{19}$$

(3) Concerning the third boundary condition, r^* may be determined by the knowledge, at a fixed radius r', of the function $T(r', z)$. Unfortunately, it is unknown and extremely difficult to detect experimentally because of the small water thickness in which the temperature gradient is concentrated. As a consequence, r^* will be determined from the knowledge of experimental data for low inlet water mass flow rate. With P the thermal power exchanged over the surface S

$$P = \int_S -\left(K\frac{\partial T}{\partial z}\bigg|_{z=0}\right)ds$$

$$= \frac{2KTr^{*2}}{z^*}\sqrt{\pi}\left(\sqrt{\left(\left(\frac{R^2 - r_o^2}{r^{*2}}\right)^2 + 1\right)} - 1\right). \tag{20}$$

With reference to the experimental run characterized by

$$T_v = 106.0°C \quad W_i = 3.33\,g\,s^{-1}$$
$$T_u = 27.5°C \quad b = 7.5\,mm$$
$$T_i = 17.5°C \quad P = 140.4\,W$$

the integration constant r^* assumes the value 0.0313 m.

The final expression of the thermal field, with this value of r^*, is given by

$$T(r, z) = T\left(1 - \frac{2}{\sqrt{\pi}}\int_0^g e^{-u^2}\,du\right). \tag{21}$$

Remembering the introductory remarks and the adopted procedure for the determination of r^*, the thermal field represented by equation (21) is strictly valid only for water laminar flow in the reversal region. The extension of the model validity to higher water velocities and then to water turbulent flow in the reversal region (heat transfer region) will now be discussed.

For a flowing fluid with a thermal gradient normal to the direction of the flow, the heat flux is due not only to the thermal conductivity but also to the turbulent transport.

Bird *et al.* [15] suggested that the phenomenon be described by means of the so-called 'turbulent conductivity'.

For a fluid in turbulent motion, the turbulent component to the heat flux may be analogously expressed in the form

$$q_{turb} = -K_{turb}\,\mathrm{grad}\,(T)$$

where K_{turb}, the value of which may be much higher than K, can be obtained by means of experimental correlations, for instance, of the Dittus—Boelter type (see Appendix C)

$$K_{turb} = (a_1 Re^{a_2} Pr^{a_3})K. \tag{22}$$

So, replacing in the thermal field equation the molecular conductivity, K, with the expression

$$K_t = K + K_{turb} \tag{23}$$

equation (21) can be employed to describe the thermal field in the reversal region also for water in turbulent motion.

A 'trial and error' method, coupled with a least-square fitting through all the experimental data (see Appendix C), yields a_1, a_2 and a_3 together with the new, actual value of r^*

$$a_1 = 6.4 \times 10^{-5}, \quad a_2 = 1.85$$
$$a_3 = 2.21, \quad r^* = 0.044. \tag{24}$$

So, finally, the thermal field in the reversal region can be expressed by

$$T(r, z) = T\left(1 - \frac{2}{\sqrt{\pi}}\int_0^g e^{-u^2}\,du\right) \tag{21}$$

with

$$g = \frac{z}{z^*} \frac{(R^2 - r^2)/r^{*2}}{\sqrt{\left(\left(\frac{R^2 - r^2}{r^{*2}}\right)^2 + 1\right)}} \quad (15)$$

and

$$z^* = \sqrt{\beta} = \sqrt{\left(\frac{K}{\rho c_p v_o}\right)}, \quad v_o = \frac{W_i}{2\pi b \rho (R^2 - r_o^2)} \quad (25)$$

where K_t and r^* are calculated by means of equations (22)–(24).

6. MODEL PREDICTIONS

Remembering equation (20), the total heat transfer coefficient (integral value) is given by

$$h_t = \frac{P}{S(T_v - T_i)} = \frac{2K_t r^{*2}}{Sz^*} \sqrt{\pi} \left(\sqrt{\left(\left(\frac{R^2 - r_o^2}{r^{*2}}\right)^2 + 1\right)} - 1\right). \quad (26)$$

As far as the water outlet temperature is concerned, its value can be provided by equation (21) as a weighted average over the reversal region thickness, b, at the discharge radius, r_o

$$T_m = \int_0^b \frac{T(r_o, z)}{b} dz = \int_0^b \frac{T}{b} \left(1 - \frac{2}{\sqrt{\pi}} \int_0^{g(r_o)} e^{-u^2} du\right) dz. \quad (27)$$

To take into account the distortion of the thermal field close to the discharge channel, which may appreciably deviate the actual outlet temperature, T_o from the estimated T_m, it is necessary to denote an aspect factor, f_f, so that

$$T_o - T_i = f_f T_m.$$

The aspect factor, f_f, has been determined with the above-mentioned trial and error method ($f_f = 0.32$) and so the actual outlet water temperature, T_o, is given by the expression (see Appendix B)

$$T_o - T_i = 0.257 \frac{z^*}{b} \frac{\sqrt{\left(\left(\frac{R^2 - r_o^2}{r^{*2}}\right)^2 + 1\right)}}{(R^2 - r_o^2)/r^{*2}} \quad (28)$$

A comparison between the total heat transfer coefficient computed by equation (26) and experimental data is proposed in Fig. 5. Most data lie in a ± 25% band, which also represents the confidence level of experiments (from error propagation analysis). A different representation is given in Fig. 6 in which experimental and computed heat transfer coefficients are plotted vs inlet water mass flow rate.

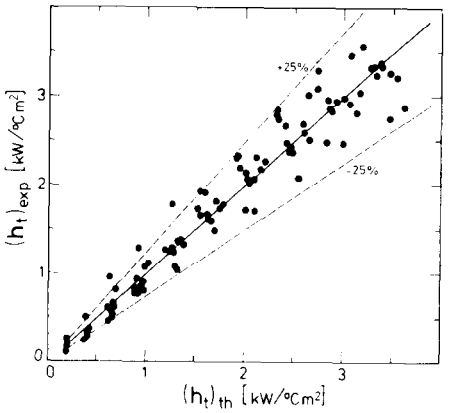

FIG. 5. A comparison between the total heat transfer coefficient from experimental data and model predictions.

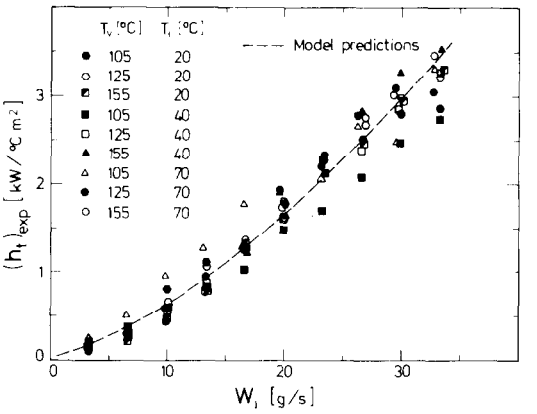

FIG. 6. Total heat transfer coefficient vs inlet water mass flow rate: experimental data and model predictions.

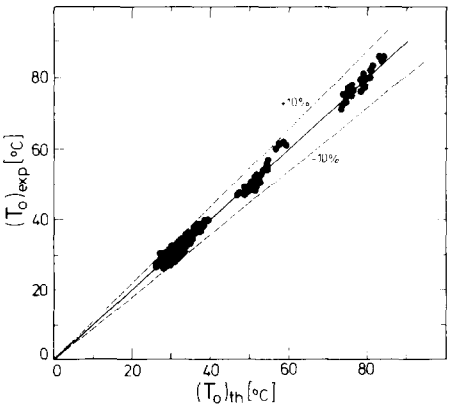

FIG. 7. A comparison between outlet water temperature from experimental data and model predictions.

In Fig. 7 a comparison between computed and experimental outlet water temperature data shows a

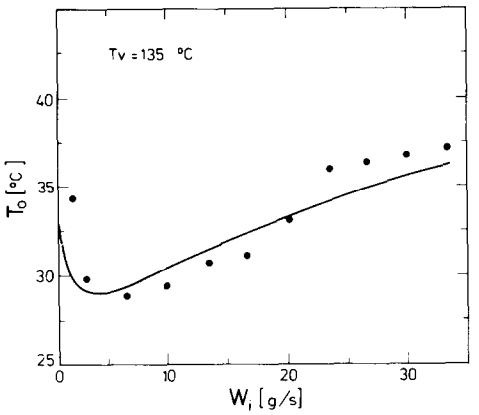

FIG. 8. Outlet water temperature vs inlet water mass flow rate.

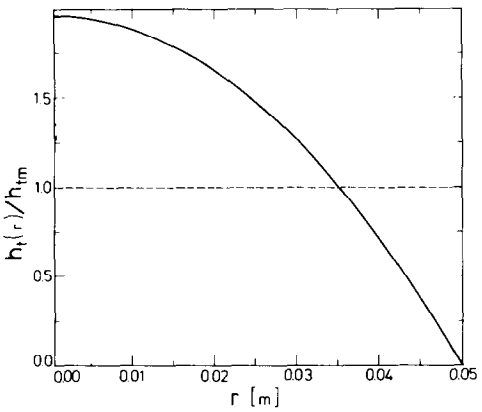

FIG. 9. Prediction of the local total heat transfer coefficient, referred to the value at the average radius, vs the distance from the exit.

fine agreement well within a ± 10% band. Also the trend of outlet water temperature vs inlet water mass flow rate is reasonably well predicted, as shown in Fig. 8.

The model enables also an estimation of the local heat transfer coefficient

$$h_t(r) = \frac{2K_t}{z^*\sqrt{\pi}} \frac{(R^2 - r^2)/r^{*2}}{\sqrt{\left(\left(\frac{R^2 - r^2}{r^{*2}}\right)^2 + 1\right)}}. \quad (29)$$

In Fig. 9 the local total heat transfer coefficient, $h_t(r)$, referred to the value computed at the mean radius, $\bar{r}$, is plotted vs the radius of the pool (see Appendix B).

Finally, the prediction of the heat transfer coefficient vs the reversal region thickness, b, shown in Fig. 10, is in good agreement with the experimental data, confirming the validity of the adopted fluid-dynamics model. The direct contact condensation heat transfer coefficient is obtained by

$$h_c = \frac{h_t}{(1 + (H_{lsat} - H_o)/\lambda)} \quad (10)$$

and the agreement with experimental data is completely similar to the prediction of h_t, as shown in Fig. 11.

7. CONCLUDING REMARKS

With reference to an experiment previously carried out by the authors [14], a theoretical model is presented for the prediction of the direct contact condensation between saturated steam (in quasi-stagnant condition) and subcooled, slowly moving water.

The precision of the model is within the experimental accuracy for the prediction of both the heat transfer coefficient and the outlet water temperature.

The model is very easy to apply, requiring only the use of a pocket computer.

Although the model has been developed for a cylindrical geometry, its extension to other geometries is easy and will be accomplished in the near future for the plane geometry, together with *ad hoc* experiments.

Acknowledgements—The authors wish to express their gratitude to Mrs B. Perra for assistance in editing this paper.

REFERENCES

1. S. G.Bankoff and H. J. Kim, Countercurrent steam–water flow in a flat plat geometry, Rept Nu-8201B, Chem. Engng Dept., Northwestern University, Evanston, Illinois (1982).
2. S. G. Bankoff and H. J. Kim, Local heat transfer coefficients for condensation in stratified countercurrent steam–water flows, ASME Paper No. 82-WA/HT-24 (1982).
3. S. G. Bankoff and H. J. Kim, Local condensation rate in nearly horizontal stratified countercurrent flow of steam and cold water, *A.I.Ch.E. Symp. Ser.* 225, **79**, 209–223 (1983).
4. L. K. Brumfield, R. N. Houze and T. G. Theofanus, Turbulent mass transfer at free, gas–liquid interfaces with application to open channel, bubble and jet flows, *Int. J. Heat Mass Transfer* **19**, 613–624 (1976).
5. L. K. Brumfield, R. N. Houze and T. G. Theofanus, Turbulent mass transfer at free, gas–liquid interfaces, with application to film flows, *Int. J. Heat Mass Transfer* **18**, 1077–1081 (1975).
6. J. H. Linehan, The interaction of two-dimensional stratified, turbulent air–water and steam–water flows, Ph.D. thesis, Dept. of Mech. Engng, University of Wisconsin (1968).
7. R. M. Thomas, Condensation of steam on water in turbulent motion, *Int. J. Multiphase Flow* **5**, 1–15 (1979).
8. W. Kirchner and S. G. Bankoff, Condensation effects in reactor transients, *Nucl. Sci. Engng* **89**, 310–321 (1985).
9. J. A. Block, Condensation-driven fluid motions, *Int. J. Multiphase Flow* **6**, 113–129 (1980).

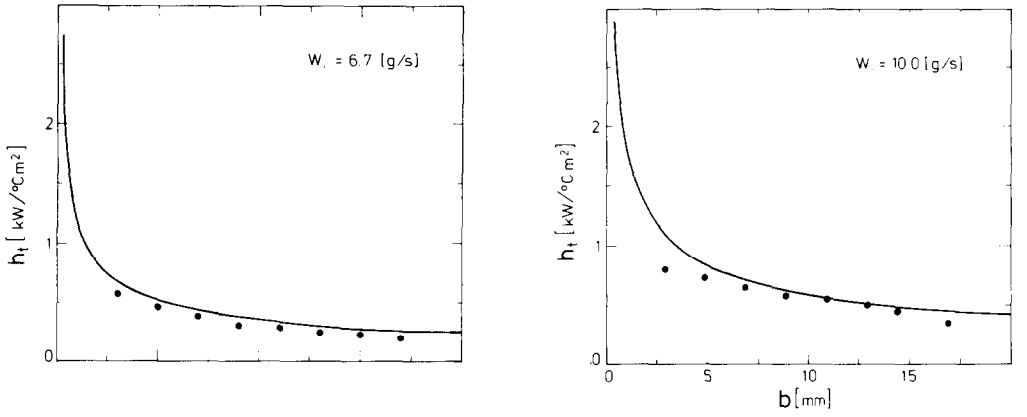

FIG. 10. Total heat transfer coefficient vs the reversal region thickness, for two different inlet water mass flow rates: experimental data and model predictions.

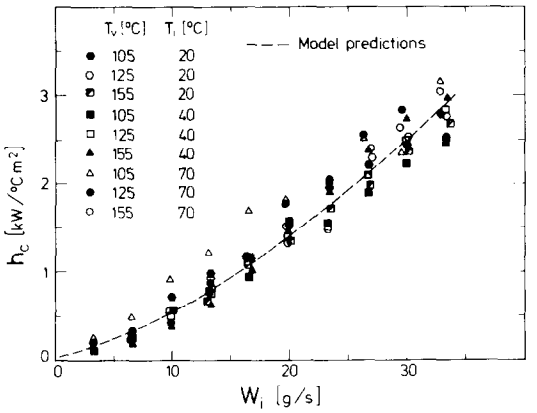

FIG. 11. Direct contact condensation heat transfer coefficient vs inlet water mass flow rate: experimental data and model predictions.

10. D. H. Rooney, H. C. Simpson, A. M. Bradford and E. W. Bessada, Non-equilibrium effects in direct contact condensation under countercurrent flow, European Two-phase Flow Group Meeting, Eindhoven, 2–5 June (1981).
11. D. H. Rooney and H. C. Simpson, Further studies of non-equilibrium during refill in a PWR, European Two-phase Flow Group Meeting, Zurich, 14–17 June (1983).
12. S. G. Bankoff, Some condensation studies pertinent to LWR safety, *Int. J. Multiphase Flow* **6**, 51–67 (1980).
13. E. M. Sparrow and J. L. Gregg, A boundary layer treatment of laminar film condensation, *J. Heat Transfer* **21**, 13–18 (1969).
14. G. P. Celata, M. Cumo and G. E. Farello, Direct contact condensation of steam on slowly moving water, III International Topical Meeting on Reactor Thermal Hydraulics, Newport, Rhode Island, 15–18 October (1985).
15. R. B. Bird, W. E. Stewart and E. N. Lightfoot, *Transport Phenomena*. Wiley, New York (1960).
16. G. Focardi, Analisi Teorico-Sperimentale della Condensazione per Contatto Diretto in Regime di Transizione Laminare.—Turbolento, Tesi di Laurea in Ingegneria Nucleare, University of Rome (1985), in Italian.

APPENDIX A

The physical properties of water may be computed at a reference temperature

$$T_r = \frac{T_{sat} + T_b}{2}.$$

As far as Reynolds number is concerned

$$Re = \frac{\rho_r \bar{v} \bar{D}_{eq}}{\mu_r}$$

the average radial velocity, $\bar{v}$, and the average equivalent diameter, $\bar{D}_{eq}$, referring to a hollow cylinder whose external diameter is the pool inner diameter, $D = 100$ mm, whose inner diameter is the discharge channel outer diameter, $D_o = 15$ mm, and whose height is the difference in level between the water surface and the discharge channel, $b = 7.5$ mm (see Fig. 2), may be computed as

$$\bar{D}_{eq} = \frac{4A(\bar{r})}{P(\bar{r})} = \frac{4\pi \bar{r} b}{2\pi \bar{r} + b}$$

with

$$\bar{r} = \frac{2\pi}{S} \int_{D_o/2}^{D/2} r^2 \, dr$$

giving $\bar{r} = 34$ mm and $\bar{D}_{eq} = 14.5$ mm.

For the average velocity, $\bar{v}$, considering the mass conservation equation

$$W_i \frac{R^2 - r^2}{R^2 - r_o^2} = \rho_r A(r) v(r)$$

with $R = D/2$ and $r_o = D_o/2$. Solving with respect to $v(r)$

$$v(r) = \frac{W_i}{2b\pi\rho_r} \left[\frac{1}{R^2 + r_o^2}\right] \left[\frac{R^2}{r} - r\right]$$

$$\bar{v} = \frac{2\pi}{S} \int_{D_o/2}^{D/2} v(r) r \, dr$$

and finally

$$\bar{v} = 460 \frac{W_i}{\rho_r} (\mathrm{m\,s^{-1}})$$

where ρ_r is the water density.

APPENDIX B

Concerning the solution of the integral in equation (27)

$$T_m = \int_0^b \frac{T(r_o, z)}{b} dz = \int_0^b \frac{T}{b}\left(1 - \frac{2}{\sqrt{\pi}}\int_0^{g(r_o)} e^{-u^2} du\right) dz$$

it is possible to notice that the expression

$$\frac{1}{\sqrt{\pi}}\int_0^g e^{-u^2} du$$

is the integral of a normalized Gaussian distribution with $\sigma^2 = 1/2$.

From the solving tables of Gaussian integrals we have, for $g = 2.9\sigma - 2.05$

$$T(\delta_z, r_o) = 0.0038T \approx 0$$

where δ_z is the value of z for which

$$g(\delta_z, r_o) = 2.05.$$

We will, therefore, have

$$T(z, r_o) \simeq 0 \text{ for } z > \delta_z.$$

With the test verifying

$$\delta_z \leqslant b$$

we can write

$$T_m = \frac{1}{b}\int_0^{\delta_z} T\left(1 - \frac{2}{\sqrt{\pi}}\int_0^g e^{-u^2} du\right) dz.$$

The Gaussian integral tables give the solution

$$T_m = 0.57\frac{z^*}{b} T \frac{\sqrt{\left(\left(\frac{R^2 - r_o^2}{r^{*2}}\right)^2 + 1\right)}}{(R^2 - r_o^2)/r^{*2}}.$$

APPENDIX C

According to ref. [15] K_{turb} can be calculated by means of a relation of the type

$$K_{turb} = K(a_1 Re^{a_2} Pr^{a_3}). \quad (22)$$

For a pipe flow

$$q = h\Delta T = K_{turb}\frac{\partial T}{\partial r}$$

where ΔT is the temperature difference between the wall and the bulk fluid, and $\partial T/\partial r$ is the mean value of the thermal gradient.

If D is the characteristic length of the heat transfer process (e.g. the hydraulic diameter), $\Delta T/D$ is evidently an estimation of the mean gradient $\partial T/\partial r$.

Introducing the Nusselt number, Nu, the following equations can be written

$$Nu = \frac{hD}{K} = \frac{h\Delta T}{K\Delta T/D} = \frac{K_{turb}\partial T/\partial r}{K\partial T/\partial r} = \frac{K_{turb}}{K}.$$

Finally equation (22) is obtained if the Nusselt number is expressed, as usual, as a function of Reynolds and Prandtl numbers.

Concerning the outlet water temperature we can write (see also Appendix B)

$$T_o - T_i = 0.57 f_f \frac{T\sqrt{\left(\left(\frac{R^2 - r_o^2}{r^{*2}}\right)^2 + 1\right)}}{(R^2 - r_o^2)/r^{*2}} \sqrt{\left(\frac{K_t}{\rho c_p v_o}\right)}.$$

Starting from the value of r^* obtained for laminar flow as a first approach (0.0313), a least-square fitting through the experimental data of $T_o - T_i$ yields a first set of f_f, a_1, a_2 and a_3 values. A trial and error method, involving the previous equation and

$$p = \frac{2K_t T r^{*2}}{z^*}\sqrt{\pi}\left(\sqrt{\left(\left(\frac{R^2 - r_o^2}{r^{*2}}\right)^2 + 1\right)} - 1\right)$$

gives, with a quick convergence, the final values of r^*, f_f, a_1, a_2 and a_3 reported in the text.

MODELE THEORIQUE DE LA CONDENSATION PAR CONTACT DIRECT SUR SURFACE HORIZONTALE

Résumé—Un modèle théorique de condensation par contact direct est présenté pour une géométrie cylindrique et l'interaction entre la vapeur d'eau saturante et de l'eau froide en écoulement lent horizontal. Un bon accord est constaté entre les prédictions théoriques et les données expérimentales aussi bien pour le coefficient de transfert thermique que pour la température de sortie de l'eau.

EIN THEORETISCHES MODELL FÜR DIE DIREKTKONTAKT-KONDENSATION AN EINER HORIZONTALEN OBERFLÄCHE

Zusammenfassung—Unter Einbeziehung der Wechselwirkung zwischen gesättigtem Dampf und langsam fließendem, unterkühltem Wasser mit horizontaler Oberfläche wird ein theoretisches Modell der Direktkontakt-Kondensation für zylindrische Geometrie vorgelegt. Es wird eine gute Übereinstimmung zwischen Berechnung und experimentellen Daten festgestellt, sowohl für den Wärmeübergangskoeffizienten als auch die Austrittstemperaturen.

ТЕОРЕТИЧЕСКАЯ МОДЕЛЬ КОНДЕНСАЦИИ НА ГОРИЗОНТАЛЬНОЙ ПОВЕРХНОСТИ ПРИ ПРЯМОМ КОНТАКТЕ

Аннотация—Предложена теоретическая модель конденсации насыщенного пара, обладающая цилиндрической симметрией. В модели учитывается тепломассообмен между паром и недогретой медленно движущейся в горизонтальном направлении водой. Получено хорошее совпадение расчетных и экспериментальных данных для коэффициента теплообмена и температуры воды на выходе.